PHYSICAL REVIEW B **80**, 220402(R) (2009)

Multiferroicity and spiral magnetism in $FeVO_4$ with quenched Fe orbital moments

A. Daoud-Aladine,[1,*] B. Kundys,[2] C. Martin,[2] P. G. Radaelli,[1,3] P. J. Brown,[4] C. Simon,[2] and L. C. Chapon[1]
[1]*ISIS facility, Rutherford Appleton Laboratory, STFC, Chilton, Didcot, Oxfordshire OX11 0QX, United Kingdom*
[2]*Laboratoire CRISMAT-UMR, 6508 ENSI CAEN, 6, Marechal Juin, 14050 Caen, France*
[3]*Department of Physics and Astronomy, University College London, Gower Street, London WC1E 6BT, United Kingdom*
[4]*Institut Laue-Langevin, 6 rue Jules Horowitz, BP 156, 38042 Grenoble Cedex 9, France*
(Received 27 October 2009; published 7 December 2009)

$FeVO_4$ has been studied by heat capacity, magnetic susceptibility, electric polarization and single-crystal neutron-diffraction experiments. The triclinic crystal structure is made of *S*-shaped clusters of six Fe^{3+} ions, linked by VO_4^{3-} groups. Two long-range magnetic ordering transitions occur at $T_{N1}=22$ K and $T_{N2}=15$ K. Both magnetic structures are incommensurate and below T_{N2}, $FeVO_4$ becomes weakly ferroelectric coincidentally with the loss of the collinearity of the magnetic structure in a very similar fashion than in the classical $TbMnO_3$ multiferroic material. However we argue that the symmetry considerations and the mechanisms invoked to explain these properties in $TbMnO_3$ do not straightforwardly apply to $FeVO_4$. First, the magnetic structures, even the collinear structure, are all acentric so that ferroelectricity in $FeVO_4$ is not correlated with the fact magnetic ordering is breaking inversion symmetry. Regarding the mechanism, $FeVO_4$ has quenched orbital moments that questions the exact role of the spin-orbit interactions.

DOI: 10.1103/PhysRevB.80.220402 PACS number(s): 75.25.+z, 77.80.−e, 25.40.Dn

There has been a recent surge of interest in a certain class of magnetoelectric materials,[1] the type-II multiferroics, where ferroelectricity arises below a magnetic phase transition as a direct consequence of complex magnetic ordering.[2] The phenomenon results from lowering of the magnetocrystalline symmetry to a polar group, and it is indeed found in compounds fulfilling strict magnetostructural symmetry requirements.[3,4] It typically appears in systems subjected to magnetic frustration or strong exchange competition, as in $Ni_3V_2O_8$ (Ref. 3) or $TbMnO_3$.[4,5]

Besides symmetry considerations, type-II multiferroics must possess a microscopic mechanism to generate electric-dipole moments. A variety of such mechanisms have been proposed:[6] magnetostriction is the only allowed mechanism for acentric collinear structures, and is active in the Ising system $Ca_3(Co,Mn)_2O_6$ (Ref. 7) and, most likely, in the commensurate phase of YMn_2O_5.[8] Most other "type-II" multiferroics are cycloidal magnets, where noncollinear spins are key ingredients in the context of the so-called spin-current model.[9,10] For this, a crucial role is played by relativistic spin-orbit interaction, which can take place at the ligand ionic site, as for pure e_g systems, within the transition-metal t_{2g} orbitals or between t_{2g} and e_g orbitals.[6] A particularly interesting case of the latter is provided by high-spin d^5 systems ($S=5/2$) where $L=0$ in the free ion and the orbital angular momentum is supposedly absent. As for the acentric and noncollinear magnetic structure itself, antisymmetric spin exchange brought by spin-orbit interactions becomes important in materials having a connected network of strong *symmetric* exchange interactions such as superexchange (SE) interactions, which can be destabilized by the presence of either strong next-nearest-neighbor interactions or by geometrical frustration.[1,11]

In this Rapid Communication, we describe a multiferroic compound—$FeVO_4$—in which the magnetic ion is orbitally quenched Fe^{3+} (d^5, $L=0$, $S=5/2$). The magnetic and dielectric phase diagram of $FeVO_4$, as determined from magnetization, specific-heat and neutron-diffraction measurements, is that of a typical cycloidal magnet: ferroelectricity appears below $T_{N2}=15$ K, coinciding with the appearance of a noncollinear incommensurate magnetic structure (phase II), whereas a second collinear incommensurate magnetic phase (I), stable between $T_{N1}=22$ K and T_{N2}, is not ferroelectric. Uniquely, $FeVO_4$ does not contain connected magnetic direct-exchange or SE paths, and the magnetic modulation is primarily determined by a network of super-super-exchange (SSE) interactions. These pathways form loops connecting an odd number of Fe^{3+}, suggesting that frustration plays a key role in promoting noncollinearity and ferroelectricity.

Polycrystalline samples and single crystals were prepared following the procedures described in Refs. 12 and 13. Electric measurements and specific-heat and magnetic-susceptibility measurements were carried out on dense pellets of polycrystalline $FeVO_4$ using a physical properties measurement system Quantum design cryostat. The electrical polarization was derived from integration of the pyroelectric current measured with a Keithley 6517 electrometer. Magnetization measurements on single crystals were made with a vertical-field superconducting quantum interference device magnetometer using a horizontal axis sample rotator. Single-crystal neutron nuclear and magnetic Bragg-peak intensities were collected and at $T=2$ K and $T=18$ K on the four-circle diffractometer D15 ($\lambda=1.174$ Å) at the Institut Laue-Langevin (ILL), France. All the nuclear and magnetic structure refinements were carried out with the program FULLPROF.[14]

The crystal structure of $FeVO_4$ is shown in Fig. 1. To facilitate the description of the magnetic structures (see below) we have redefined the triclinic basis vector $\mathbf{c}$ so that $\mathbf{c}=-2\mathbf{a}'-\mathbf{c}'$, where $\mathbf{a}'$ and $\mathbf{c}'$ are the basis vectors used in Ref. 13. The important crystallographic features for the description of the magnetic properties are easily identified. The Fe^{3+} ions, all in the high-spin state $S=5/2$ (see below), are arranged in clusters, separated by $(VO_4)^{3-}$ groups, containing nonmagnetic V^{5+} ions. Each cluster of 6 Fe^{3+} ions consists of two identical Fe_3O_{13} monomers, related by a center of inver-

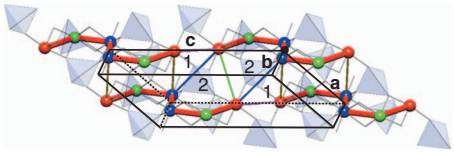

FIG. 1. (Color) (a) Crystal structure and magnetic exchange frustration in $FeVO_4$. The basic magnetic unit are *S*-shaped clusters made of six Fe^{3+} atoms (red, blue, and green large balls) well spaced by $V^{5+}O_4$ tetrahedra (blue). The Fe-O bonds are drawn as thin gray lines (O atoms are not shown for clarity). The thick red lines represent intracluster interactions, with contributions from direct Fe-Fe exchange and Fe-O-Fe superexchange. Iron atoms belonging to different clusters are coupled by Fe-O-O-Fe SSE paths mediated by the edges of the VO_4^{3-} tetrahedra giving rise to effective intercluster Fe-Fe interactions (thin colored lines).

sion. With our convention, the **c** axis runs along the line connecting adjacent clusters through their centers and open ends. In Fig. 1, we have also represented the two main types of magnetic interactions: intracluster direct-exchange and SE interactions (thick lines), which are antiferromagnetic (AF), and intercluster SSE interactions (thin lines). There is clearly the potential for magnetic frustration, since Fig. 1 reveals that the effective intercluster and intracluster Fe-Fe linkages form loops (labels 1 and 2), which contain an odd number of Fe sites, within which collinear AF arrangements cannot be fully satisfied.

The magnetic frustration and competition between SE and SSE interactions give rise to a complex low-temperature phase diagram, reminiscent of that of other cycloidal magnets. Above 100 K the magnetic susceptibility follows a Curie-Weiss law (not shown). The effective paramagnetic moment $\mu_{eff}=6.103(4)\mu_B$ is near the value expected for Fe^{3+} ions in the high-spin $S=5/2$ state ($\mu_{eff}^{th}=5.91\mu_B$). The Weiss temperature $\theta_{CW}=-124.9(4)$ K confirms the presence of strong AF interactions. The low-temperature data clearly indicate magnetic transitions at $T_{N1}=22$ K and $T_{N2}=15$ K, consistent with a frustration index of $|\theta_{CW}|/T_{N1}\sim 6$. The specific heat [Fig. 2(a)] also shows two lambda-type anomalies at these critical temperatures. The magnetic contribution to the specific heat was determined by subtracting the lattice contribution, indicated by the dashed line in Fig. 2(a), which was estimated by fitting the data at high temperature to the Debye function [Debye temperature of 385(5) K]. The magnetic entropy integrated between 2 and 50 K is $S_M=13.98$ J K^{-1} mol^{-1}, approaching the classical value of $R\log(2S+1)=14.89$ J K^{-1} mol^{-1} for $S=5/2$. A large fraction of the total magnetic entropy ($\sim$30%) is only recovered far above T_{N1}, indicative of short-range AF ordering above T_{N1}.[15]

To obtain further insight into the nature of the magnetic ordering taking place at T_{N1} and T_{N2}, magnetic measurements were made on a needle-shaped single crystal. The crystal orientation was set at 300 K before cooling the crystal in a field of 3 T and recording magnetization data between 5 and 35 K. At low temperatures, the direction of minimal susceptibility coincides with the direction of growth of the needle-shaped crystals (approximately along the crystallographic direction **a**). With this field orientation, labeled $\mathbf{H}_{\|}$ in

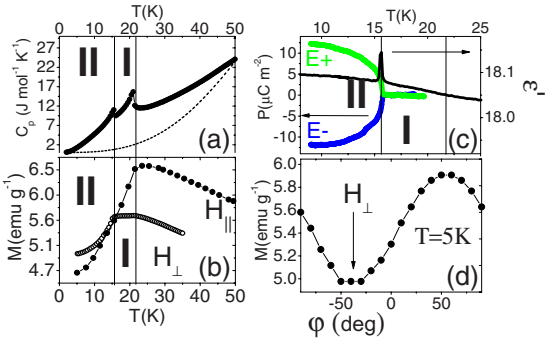

FIG. 2. (Color online) Magnetoelectric phase diagram for $FeVO_4$. (a) Heat capacity (filled circles). The dashed line shows the estimated lattice Debye contribution (see text for details) (b) Single crystal magnetization at 3 T with the magnetic field applied in the directions $\mathbf{H}_{\|}$ (filled circles) and $\mathbf{H}_{\perp}$ (opened circles) explicated in the panel (e). (c) Bulk electric polarization measured for a sample cooled in a positive [*E*+, green (light gray)] and negative [*E*−, blue (black)] electric field of 160V and dielectric constant (black solid line). (d) Angular dependence of the magnetization at 3 T and $T=5$ K measured varying the orientation of the applied magnetic field in the ($\mathbf{b}^*$,$\mathbf{c}^*$) plane. **H** is aligned with $\mathbf{c}^*$ when $\phi=0$.

Fig. 2(b), one only observes the magnetic transition at T_{N1}. The transition at T_{N2} is clearly visible in measurements with the field applied *perpendicular* to the **a** axis, i.e., in the $\mathbf{b}^*$-$\mathbf{c}^*$ plane. By rotating the crystal around its needle axis, we have determined the secondary easy magnetic directions in this plane. This is shown in Fig. 2(d). The minimum and maximum of the magnetization were found for the crystal rotated $\phi_{min}=-40°$ and $\phi_{max}=50°$ away from the $\mathbf{c}^*$ direction, respectively. The temperature dependence of the magnetization with the field orientation ϕ_{min}, labeled as $\mathbf{H}_{\perp}$ in Fig. 2(b) shows a pronounced drop below T_{N2}.[16] The phase boundaries indicated in Fig. 2 therefore mark the domains of stability of two distinct magnetic phases (I and II). The temperature dependence of the dielectric susceptibility, shown in Fig. 2(c), has no anomaly at T_{N1} but the sharp peak at T_{N2} and the concomitant appearance of an electrical polarization [Fig. 2(c)] demonstrates that the system becomes ferroelectric in phase II, while phase I is not ferroelectric. The value of the electrical polarization at low temperatures is 1 order of magnitude smaller than for $TbMnO_3$,[5] a large reduction which can be partly attributed to the fact that our dielectric measurements were made on polycrystalline samples.

The magnetic structures of phases I and II were determined by single-crystal neutron diffraction. Below T_{N1}, the data show Bragg peaks of magnetic origin, which can all be indexed with a single, nearly temperature-independent propagation vector $\mathbf{k}=(0.222-0.089\ 0.012)$ almost perpendicular to **c**. In the most general case of a single-**k** incommensurately modulated structure, the magnetic moments $\mathbf{M}_j(\mathbf{R}_l)$ on a given crystallographic site describe an ellipse as they propagate in different unit cells $\mathbf{R}_l$. $\mathbf{M}_j(\mathbf{R}_l)$ can therefore be written as

$$\mathbf{M_j}(\mathbf{R_l}) = \mathbf{A_j}\cos(2\pi\,.\,\mathbf{k}\cdot\mathbf{R_l}+\varphi_j) + \mathbf{B_j}\sin(2\pi\,.\,\mathbf{k}\cdot\mathbf{R_l}+\varphi_j) \quad (1)$$

where $\mathbf{A}_j$ and $\mathbf{B}_j$ are two perpendicular vectors defining the major and minor semiaxes of the ellipse.[18] An initial set of

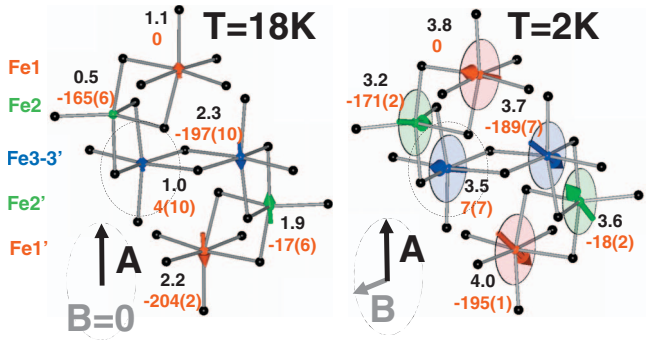

FIG. 3. (Color) Zoom in on the magnetic order of the Fe *S*-shaped cluster of Fig. 4 containing the surrounded spin. The three inequivalent Fe sites are shown as small red, green, and blue spheres, and the Fe sites with primed labels are obtained by inversion symmetry. The Fe are arranged in two types of edge-sharing polyhedra: two $Fe^{3+}O_5$ trigonal bypiramids (sites 2-2′) and the four other sites in $Fe^{3+}O_6$ octahedra. Spin are aligned with a common direction **A** at $T=18$ K, and rotate in the same (**A**,**B**) plane at $T=2$ K. The magnetic-moment amplitudes (black labels) were calculated using Eq. (1) with the refined parameters given in the supplementary information (Ref. 17), accounting for a dephasing term of 68.4° coming from the position of the cluster in the crystal [$\mathbf{R}_{//}=(0\ \bar{2}\ 1)$]. Only the values of the refined phases φ_j are given in degrees (red labels) for clarity.

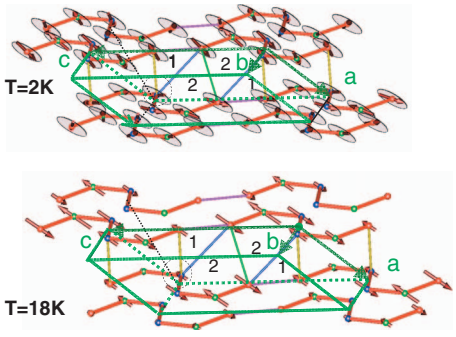

FIG. 4. (Color) Magnetic structure of $FeVO_4$ as derived from refinements of the single-crystal neutron-diffraction data $T=2$ K (top) and $T=18$ K (bottom). The magnetic moments are shown as brown arrows. For the noncollinear structure at 2 K, the envelop of the helicoidal modulation is also shown by gray ellipses at each lattice site. Frustrated exchange loops are reproduced from Fig. 1, and one spin on loop 1 experiencing the geometrical exchange frustration is surrounded.

refinements indicated that the magnetic structure of phase I is a *collinear* spin-density wave (i.e., $\mathbf{B}_j=0$), whereas phase II possesses a *helical* structure. It is noteworthy that the collinear direction of the spins in phase I coincides with the major semiaxis $\mathbf{A}_j$ of the ellipses in phase II, indicating that the spin anisotropy does not change at the phase boundary. In principle, both the amplitudes and directions of $\mathbf{A}_j$ and $\mathbf{B}_j$ as well as the phase angles of the modulations can be different for each site. We have shown that the correlation between parameters can be significantly reduced by introducing constraints[17] while still yielding refinements of excellent quality. This has lead us to consider only minimal models for phase I (10 parameters, $R_{F2}=10.3\%$ and $\chi^2=1.7$) and phase II (14 parameters, $R_{F2}=5.07\%$ and $\chi^2=8.2$). The constraints retained suggest that the data do not support significantly different orientations of the ellipses and that the amplitudes $|\mathbf{A}_j|$ and $|\mathbf{B}_j|$ (Fig. 3) of atoms related by centrosymmetry do not differ significantly, although their phases are not related by centrosymmetry and need to be determined independently. Perspective views of the magnetic structures of phases I and II are shown for one cluster in Fig. 3 and for few clusters in Fig. 4.

At $T=2$ K, the helical magnetic order reveals different degree of frustration in different directions. It is characterized by the presence of quasi-1D AF order on chains of S-shaped clusters running in the **c** direction. The SSE path linking clusters in this direction is therefore probably the least frustrated SSE interaction inducing only very slow rotations of the average AF direction over a very long period of approximately 110 nm. This contrasts with all the other SSE paths, which induce large rotations of the average AF direction between neighboring chains.

Noteworthy is that all the magnetic orders, including the collinear phase I, are acentric. The acentric nature directly comes from the phase difference for each pairs of sites related by inversion symmetry, which all significantly deviate from 180° (Fig. 3). This inversion symmetry breaking is obvious at $T=2$ K, and the phases are such that each half cluster of 3 Fe shows an almost perfect AF order, but between the two halves, the AF directions are canted by $15\sim20°$. As similar phases are refined at $T=2$ K and $T=18$ K, the collinear magnetic order at $T=18$ K essentially appears as the projection of the helical order on the common **A** direction, which is why it is also acentric. This situation is different than in prototype cycloidal magnets $Ni_3V_2O_8$ or $TbMnO_3$, where the magnetic symmetry breaking of the inversion symmetry is claimed to be a crucial ingredient for the emergence of ferroelectric behavior and was only ascribed to the spiral phase.[3,4] Here, ferroelectricity essentially results from a transition to a noncollinear magnetic order in the ground state below T_{N2}.

The onset of a collinear order at higher temperatures has already been discussed by Mostovoy.[10] In the high-temperature regime above T_{N2}, anisotropy dominates so that the moments align along the local easy axis, whereas below, the reduction in entropy enables ordered components of moment in directions orthogonal to it. For $FeVO_4$ the local easy axis is the **A** direction deduced from the neutron data, which coincides with the macroscopic easy axis determined from the magnetization measurements and labeled $\mathbf{H}_{\|}$ in Fig. 2(b). In phase II the moments are confined to the plane of the ellipses with **A** and **B** as semiaxes, drawn in Figs. 3 and 4. When a field is applied in any direction orthogonal to **A** ($\mathbf{H}_{\|}$) the temperature dependence of the magnetization shows a singularity at T_{N2}, a rapid fall below T_{N2} and almost no singularity at T_{N1}. The orthogonal direction for which the fall is most pronounced is parallel to **B**, the minor axis of the ellipse. The noncollinearity of phase II reflects the appearance of a second-order parameter modulating moments oriented parallel to **B** stabilized by the presence of additional terms in the free energy which outweigh the entropy effect. The noncollinearity suggests that these terms are due to antisymmet-

ric spin-orbit coupling of the Dzyaloshinski-Morya-type proportional to vector products of spins $\mathbf{S}_i \times \mathbf{S}_j$. Most theories of multiferroic spiral magnets have invoked this interaction as the driving force leading to magnetically induced ferroelectricity, even if it is yet unclear if it arises from spin currents[9] or the emergence of ion displacements.[19]

In summary, we have demonstrated magnetically induced ferroelectricity in $FeVO_4$. It is noteworthy that its magnetoelectric phase diagram in the vicinity of T_{N2} is very similar to that of the classical $TbMnO_3$ system in the vicinity of $T_{lock}=27$ K.[5,20] However, there are important differences distinguishing $FeVO_4$ from known type-II multiferroic materials, which challenge the theories describing the mechanism of multiferroic behavior and the symmetry of the multiferroic state. Inverse Dzyaloshinski-Morya interactions may not be here the sole active mechanism, since the Fe^{3+} ions have $L=0$ in the free-ion state and because in $FeVO_4$ the breaking of inversion symmetry of the magnetic order occurs in both phase I and phase II, so it is not correlated with the ferroelectric properties, which appear in phase II only. Besides, $FeVO_4$ highlights better the connection between the exchange frustration and the magnetic order. In $TbMnO_3$ or $Ni_3V_2O_8$ such connection is harder to identify because the SSE interactions form a network of next-nearest-neighbor interactions interpenetrating that of the first neighbor superexchange interactions. In $FeVO_4$ we have established a clear connection between the moment reductions or the spin rotations, which are typical of the incommensurate magnetic phases of spiral magnets, and the most relevant exchange paths giving rise to the magnetic frustration.

We thank J. A. Rodriguez-Velazman for his assistance during the neutron-diffraction experiment at the ILL.

*aziz.daoud-aladine@stfc.ac.uk

[1] W. Eerenstein, N. D. Mathur, and J. F. Scott, Nature (London) **442**, 759 (2006).
[2] S.-W. Cheong and M. Mostovoy, Nature Mater. **6**, 13 (2007).
[3] G. Lawes *et al.*, Phys. Rev. Lett. **95**, 087205 (2005).
[4] M. Kenzelmann, A. B. Harris, S. Jonas, C. Broholm, J. Schefer, S. B. Kim, C. L. Zhang, S. W. Cheong, O. P. Vajk, and J. W. Lynn, Phys. Rev. Lett. **95**, 087206 (2005).
[5] T. Kimura, T. Goto, H. Shintani, K. Ishizaka, T. Arima, and Y. Tokura, Nature (London) **426**, 55 (2003).
[6] C. Jia, S. Onoda, N. Nagaosa, and J. H. Han, Phys. Rev. B **76**, 144424 (2007).
[7] Y. J. Choi, H. T. Yi, S. Lee, Q. Huang, V. Kiryukhin, and S.-W. Cheong, Phys. Rev. Lett. **100**, 047601 (2008).
[8] L. C. Chapon, P. G. Radaelli, G. R. Blake, S. Park, and S. W. Cheong, Phys. Rev. Lett. **96**, 097601 (2006).
[9] H. Katsura, N. Nagaosa, and A. V. Balatsky, Phys. Rev. Lett. **95**, 057205 (2005).
[10] M. Mostovoy, Phys. Rev. Lett. **96**, 067601 (2006).
[11] M. Fiebig, T. Lottermoser, D. Frohlich, A. Goitsev, and R. Pisarev, Nature (London) **419**, 818 (2002).
[12] L. M. Levinson and B. M. Wanklyn, J. Solid State Chem. **3**, 131 (1971).
[13] B. Robertson and E. Kostiner, J. Solid State Chem. **4**, 29 (1972).
[14] J. Rodriguez-Carvajal, Physica B **192**, 55 (1993).
[15] This observation is consistent with a strong magnetic diffuse scattering signal above T_{N2}, in neutron powder-diffraction experiments, which we also performed separately in the $T_{N1}<T<30$ K temperature range. A more detailed account of all these observations will be reported elsewhere.
[16] The measurements in all configurations ($\mathbf{H}\perp$ and $\mathbf{H}\parallel$) are in fact both sensitive to T_{N1} and T_{N2}. This is due to the fact the crystal was misaligned with the rotator axis, leading to $\sim 10°$ errors in precision for all the given directions.
[17] See EPAPS Document No. E-PRBMDO-80-R06946 for the details of the refinement procedure, the parameters, and reliability factors of the neutron-diffraction study of the magnetic structures of $FeVO_4$. For more information on EPAPS, see http://www.aip.org/pubservs/epaps.html.
[18] O. Zaharko, A. Daoud-Aladine, S. Streule, J. Mesot, P.-J. Brown, and H. Berger, Phys. Rev. Lett. **93**, 217206 (2004).
[19] H. J. Xiang, S.-H. Wei, M.-H. Whangbo, and J. L. F. Da Silva, Phys. Rev. Lett. **101**, 037209 (2008).
[20] O. Prokhnenko, R. Feyerherm, M. Mostovoy, N. Aliouane, E. Dudzik, A. U. B. Wolter, A. Maljuk, and D. N. Argyriou, Phys. Rev. Lett. **99**, 177206 (2007).